Near-infrared fluorescence imaging using organic dye nanoparticles

Near-infrared fluorescence imaging using organic dye nanoparticles

Jia Yu[a], Xiujuan Zhang[a,*], Xiaojun Hao[a], Xiaohong Zhang[b], Mengjiao Zhou[a], Chun-Sing Lee[c,*], Xianfeng Chen[c,*]

[a]Institute of Functional Nano & Soft Materials Laboratory (FUNSOM) and Jiangsu Key Laboratory for Carbon-Based Functional Materials & Devices, Soochow University, Suzhou 215123, PR China

[b]Nano-organic Photoelectronic Laboratory and Key Laboratory of Photochemical Conversion and Optoelectronic Materials, Technical Institute of Physics and Chemistry, Chinese Academy of Sciences, Beijing 100190, PR China

[c]Center of Super-Diamond and Advanced Films (COSDAF) & Department of Physics and Materials Science, City University of Hong Kong, Hong Kong SAR, PR China

*Correspondence should be sent to: xjzhang@suda.edu.cn, apcslee@cityu.edu.hk, xianfeng.chen@cityu.edu.hk

Keywords: NIR-emissive organic nanoparticles, fluorescence resonance energy transfer, *in vitro* imaging, *in vivo* imaging

Abstract

Near-infrared (NIR) fluorescence imaging in the 700-1000 nm wavelength range has been very attractive for early detection of cancers. Conventional NIR dyes often suffer from limitation of low brightness due to self-quenching, insufficient photo- and bioenvironmental stability, and small Stokes shift. Herein, we present a strategy of using small-molecule organic dye nanoparticles (ONPs) to encapsulate NIR dyes to enable efficient fluorescence resonance energy transfer to obtain NIR probes with remarkably enhanced performance for *in vitro* and *in vivo* imaging. In our design, host ONPs are used as not only carriers to trap and stabilize NIR dyes, but also light-harvesting agent to transfer energy to NIR dyes to enhance their brightness. In comparison with pure NIR dyes, our organic dye nanoparticles possess almost 50-fold increased brightness, large Stokes shifts (~250 nm) and dramatically enhanced photostability. With surface modification, these NIR-emissive organic nanoparticles have water-dispersity and size- and fluorescence- stability over pH values from 2 to 10 for almost 60 days. With these superior advantages, these NIR-emissive organic nanoparticles can be used for highly efficient folic-acid aided specific targeting *in vivo* and *ex vivo* cellular imaging. Finally, during *in vivo* imaging, the nanoparticles show negligible toxicity. Overall, the results clearly display a potential application of using the NIR-emissive organic nanoparticles for *in vitro* and *in vivo* imaging.

1. Introduction

In near-infrared (NIR) spectral range, organisms and tissues have low absorption of light and possess low intrinsic autofluorescence. Autofluorescence is the natural emission of light from biological structures. If biomarkers are fluorescent in NIR range, they can be better detected and identified from the surrounding biological environment. Therefore, NIR fluorescence imaging in wavelength range of 700-1000 nm is particularly attractive for early detection of cancers, which is expected to significantly contribute to improved cancer therapy and increased survival rates of patients [1-4].

Currently, the most widely used NIR probes are still organic dyes, which are usually encapsulated in various nanoparticles (NPs) to overcome the intrinsic limitations of conventional NIR dyes including poor hydrophilicity, low photostability, small quantum yield (QY) and instability in bio-environment [5-8]. However, most of these encapsulating nanoparticles including silica NPs, calcium phosphate NPs, and lipoprotein NPs, only act as inert carriers but do not contribute to brightness improvement of the NIR probes [9-12]. Another concern is that Stokes shift of conventional nanoparticle-based dye probes is usually small and optical interferences (light scattering and autofluorescence) caused by biosubstrates often exist, which greatly reduces detection sensitivity [13]. Furthermore, the clearance of inert carriers from patients still remains a great concern. Conjugated polymer dots (Pdots) were then reported to be utilized as the matrix to load organic dyes for imaging, in which Pdots served as light-harvesting agents to transfer their energy to organic dyes to enhance brightness [14-15].

Recently, small-molecule organic dye nanoparticles (SM ONPs) have also been developed as a new class of promising fluorescent probes [16-19], where organic dyes themselves were directly assembled into pure dye nanoparticles without nanocarriers. Despite at early stage, SM ONPs have attracted much attention, because they possess large absorption cross-sections, non-blinking property and favorable biocompatibility. More importantly, compared to Pdots, there is great variety and flexibility in materials design and thus tunability in optical properties and functionalities [20-21]. Previously,

dye molecules with rigid structures or aggregation-induced enhanced emission (AIEE) properties were used for preparing SM ONPs to avoid concentration quenching of traditional dyes [22]. For example, recently, we reported a type of ultrabright and ultrastable NIR dye nanoparticles which were prepared from a NIR dye of bis(4-(N-(2-naphthyl)phenylamino) phenyl)-fumaronitrile (NPAPF) with AIEE effect [16]. However, if traditional NIR dyes are employed to make nanoparticles, severe quenching will happen.

To address the challenges of developing NIR fluorescence probes with high brightness, large Stokes shift and photo- and bio-environmental stability, herein, we encapsulated an NIR dye into red-emissive ONPs. We hypothesize that the efficient fluorescence resonance energy transfer (FRET) from ONPs to NIR dyes will enable the resultant NPs to possess superior properties for bioimaging. To confirm this, we systematically investigated the optical properties, water-dispersity, photo- and bio-environmental stability and *in vivo* toxicity of the NIR dye doped NPs and tested their application for *in vitro* and *in vivo* imaging.

2. Experimental Section

2.1. Materials and characterization

NIR712 dye (2,9,16,23-tetra-tert-butyl-29H,31H-phthalocyanine) was purchased from Sigma Aldrich, Inc. Tetrahydrofuran (THF) was ordered from Shanghai LingFeng Chemical Reagent Co., Ltd. High-purity water (resistivity = 18.2 MΩ cm) was produced with a Milli-Q apparatus (Millipore). Fetal bovine serum (FBS), Roswell Park Memorial Institute-1640 (RPMI-1640) medium, folic acid (FA)-free RPMI-1640 and Penicillin-streptomycin solution were obtained from Invitrogen (San Diego, CA). 3-(4,5-dimethylthiazol-2-yl)-2,5-diphenyltetrazolium bromide (MTT), dimethyl sulfoxide (DMSO) and poly(maleic anhydride-alt-1-octadecene) (C18PMH) were from Sigma Aldrich (Milwaukee, WI). 4’,6-diamidino-2-phenylindole (DAPI) and LysoTracker Green DND-26 were purchased from Invitrogen. Triethylamine (TEA) and mPEG-NH_2 (5k) were from Sinopharm Chemical Reagent Co. and PegBio (Suzhou, China), respectively.

N-hydroxysuccinimide (NHS) and 1-Ethyl-3-(3-dimethylaminopropyl) carbodiimide (EDC) were ordered from Fluka. A human nasopharyngeal epidermal carcinoma cell line (KB cell), a human epithelial cervical cancer cell line (HeLa cell), a human fetal lung fibroblast MRC-5 cell line (MRC-5 cell) and a 4T1 murine breast cancer cell line (4T1 cell) were provided by American Type Culture Collection (ATCC).

UV-Vis absorption spectra were obtained on a Perkin-Elmer Lambda 750 UV/Vis/NIR spectrometer. Fluorescence spectra were measured with a Horiba Jobin Yvon luminescence spectrometer (FluoroMax 4). Scanning electron microscopy (SEM) images were taken with a FEI Quanta 200 FEG field emission scanning electron microscope. Transmission electron microscopy (TEM) images were taken by FEI Tecnai G2 F20 S-TWIN. Dynamic light scattering (DLS) measurements were carried out on a Zetasizer Nano ZS (Malvern Instruments, Malvern, U.K.). All measurements were performed at room temperature.

2.2. Synthesis of NPAFN

2,3-bis(4'-(diphenylamino)-[1,1'-biphenyl]-4-yl)fumaronitrile (NPAFN) was prepared according to previously reported procedures [23]. A mixture of 4-bromophenylacetonitrile (4.86 g, 24.8 mmol) and iodine (6.35 g, 25 mmol) was purged with N_2 and dry diethyl ether (100 mL) was injected to the mixture with a needle and syringe. Then the temperature of the solution was dropped to -78 °C. Sodium methoxide (2.84 g, 52.6 mmol) and methanol (40 mL) were subsequently slowly added within a period of over 30 min following by stirring for 40 min. Next, the solution was placed in an ice-water bath for 4 hours under stirring. Then, 3-6% hydrochloric acid was added dropwisely and the solution was filtered to separate the precipitate. After it, the precipitate was rinsed with cold methanol-water solvent and the filtrate was concentrated to obtain the second crop of product. Through these procedures, a pale yellow solid was obtained with a yield of greater than 90%.

A mixture of bis(4-bromophenyl)fumaronitrile (0.787 g, 2.03 mmol), triphenylamine (4.47 mmol), Cs_2CO_3 (1.95 g, 5.98 mmol) and toluene (13 mL) was degassed and purged with N_2. Pd/P(t-Bu)$_3$ catalyst pre-prepared from $Pd(OAc)_2$

(0.0135 g, 0.06 mmol), $P(t\text{-}Bu)_3$ (0.36 g, 0.178 mmol) and toluene (4 mL) was added to the mixture inside a glove box. The reaction mixture was then degassed, purged with nitrogen, heated to 110 °C and maintained for 24 h. The mixture was cooled to room temperature followed by adding water (30 mL) and dichloromethane (50 mL). The organic layer was separated and washed with brine, dried over anhydrous $MgSO_4$ and evaporation under reduced pressure. Finally, the product was purified by column chromatography on silica gel using 1:1 lightpetroleum/dichloromethane as eluant to afford NPAFN (1.036g) as orange solid. Melting point (°C): 249.8-250.5. ^{1}H NMR (400 MHz, $CDCl_3$, δ, ppm): 7.93 (d, 4H), 7.73 (d, 4H), 7.53 (d, 4H), 7.30 (t, 8H), 7.16 (d, 12H), 7.08 (t, 4H). ^{13}C NMR (400 MHz, $CDCl_3$, δ, ppm): 148.64, 147.43, 143.63, 132.54, 130.33, 129.94, 129.41, 129.28, 127.86, 127.67, 127.04, 126.87, 124.89, 124.01, 123.45, 123.20, 117.03, 77.23, 77.19, 77.17. MS ($C_{52}H_{36}N_4$): calcd, 716.87; found, 716.29.

2.3. Synthesis of folic acid conjugated C18PMH-PEG (C18PMH-PEG-FA)

C18PMH-PEG was synthesized as stated in literature [24]. To prepare C18PMH-PEG-FA, C18PMH-PEG was firstly functionalized with amine group. In detail, C18PMH (1eq), mPEG-NH_2 (5k) (1eq) and NH_2-mPEG(5k)-BOC (Polymere, Germany) (0.5eq) were mixed in dichloromethane under agitation. EDC (2eq) and TEA (8eq) were then added to the solution under magnetic stirring. After stirring for 24 h at room temperature, the dichloromethane solvent was blown dry with a N_2 flow. Subsequently, 2 mL of trifuoroacetic acid was added and actively stirred for 3 h at room temperature to de-protect the Boc group. After the evaporation of the TFA solvent, the residual solid was dissolved in water, which was dialyzed for 2 days in a dialysis bag (MWCO = 14 kDa) to remove unreacted PEG polymers and other reagents. After lyophilization, the final product (C18PMH-PEG-NH_2) in white solid was stored at -20 °C for future use.

The folic acid conjugated C18PMH-PEG was prepared by conjugating the amine-functionalized C18PMH-PEG-NH_2 with activated FA. Briefly, 35 mg of FA was mixed with 15 mg EDC and 23 mg NHS in 5 mL of anhydrous DMSO for 15 min

at room temperature. 20 mg of C18PMH-PEG-NH_2 in 5 mL of DMSO was added afterwards (molar ratio of NH_2/FA/EDC/NHS = 1:2:2:5). After stirring at room temperature for 8 h, water was added and the product was purified by dialysis. The final product was lyophilized and stored at -20 °C until use.

2.4. Preparation and functionalization of NIR712-doped NPs

NIR712-doped NPs were synthesized through a facile solvent exchange approach. NPAFN was first dissolved in THF to prepare a 1×10^{-3} M stock solution. Different amounts of NIR712 dye were added to 0.15 mL of the stock solutions. The mixed solutions were each injected to 5 mL of aqueous solution at 30 °C under vigorous stirring at 1000 rpm. After stirring for 3 min, the samples were stabilized for 24 hours.

For modification of NIR712-doped NPs, 2 mg of C18PMH-PEG was dispersed in 10 mL of water by sonication. Then 300 μL of solution was added into 5 mL of NPs suspensions followed by ultrasonication for 5 min. After that, solution was kept for use at room temperature. C18PMH-PEG-FA functionalization was executed referring to the former. To evaluate the stability of the NPs, evolutions of their diameter and fluorescence in phosphate buffered saline (PBS), serum and Na_2CO_3-$NaHCO_3$, Na_2HPO_4-Citric acid buffer solution of different pH values were recorded at different times. All measurements were performed at room temperature.

2.5. Determination of quantum yield

Fluorescence quantum yield was measured using a Perkin-Elmer Lambda 750 UV/Vis/NIR Spectrometer and luminescence spectrometer. We made use of 2,7-di(4-(diphenylamino)phenyl-2,1,3-benzothiadiazol-7-yl)-9,9'-spirobifluorene (Spiro-BTA) excited at 468 nm (QY = 0.45) as a standard to measure the fluorescence quantum yields of NIR712-doped NPs in suspensions. Quantum yield was calculated according to the following equation:

η, A, I and n refer to quantum yield, absorbance, fluorescent intensity and refractive indices, respectively. The subscripts s and r refer to the sample and the reference solutions respectively. In our experiments, A_r = 0.05, A_s = 0.05, n_s = 1.333 (H_2O, 20 °C), n_r = 1.4 (THF, 20 °C). It was obtained by integrating the emission spectra over 680-850 nm for NIR712-doped NPs.

2.6. Cell culture

KB cells were cultured in folic acid free RPMI-1640 and normal RPMI-1640 supplemented with 10% FBS and 1% penicillin/streptomycin solution at 37 °C in a humidified atmosphere containing 5% CO_2. The former was considered as a positive group and the latter as a negative group. 4T1 cells, MRC-5 cells and HeLa cells were cultured in normal RPMI-1640 supplemented with 10% FBS and 1% penicillin/streptomycin at 37 °C in a humidified atmosphere containing 5% CO_2.

2.7. Cytotoxicity assays

KB, MRC-5 and HeLa cell lines were grown into a 96-well cell-culture plate at 10^4-10^5/well and then incubated for 24 hours at 37 °C under 5% CO_2. After incubating the cells with different doses of NPs, the standard MTT assay was performed to measure the cell viabilities by using untreated cells as a control. In this paper, all of the error bars indicate the standard deviation (SD) of the results.

2.8. In vitro fluorescence imaging

For the FA targeted imaging experiment, both positive and negative cells were incubated with 3 μM C18PMH-PEG or C18PMH-PEG-FA modified NPs for 3 hours at 37 °C. Cells were dually labeled with blue-colored nuclei-specific DAPI and green-colored lysosome-specific Green DND-26 before observation. Confocal imaging of the cells was carried out with 488 nm laser excitation and emission was

measured from 680 to 800 nm. All cells were washed twice with cell culture medium before imaging. A flow cytometer (FACS Calibur from Becton, Dickinson and Company) was used for quantitative analysis.

2.9. In vivo fluorescence imaging

KB tumor-bearing mice were intravenously injected with 200 μL of 100 μM PEGylated NIR712-doped NPs and imaged using a Maestro *in vivo* fluorescence imaging system (CRi Inc.). The mice were excited with a blue light peaked at 455 nm. *In vivo* spectral imaging from 700 to 850 nm (10 nm step) was then carried out.

2.10. Biodistribution

Tumor-bearing mice (4T1) injected with PEGylated NIR712-doped NPs were sacrificed at 1, 6, 12, 24, and 48 hours after injection. Major organs and tumor tissue were then spectrally imaged by the Maestro system. The average intensity of the PEGylated NP fluorescence was calculated for a semi-quantitative biodistribution analysis.

2.11. Histology analysis

Untreated control mice and the mice which were injected with 200 μL of 100 μM PEGylated NIR712-doped NPs were sacrificed at Day 1, 7 and 14 after treatment. Major organs of the mice were collected, fixed in 10% of neutral buffered formalin, processed in paraffin, sectioned with a thickness of 8 μm, stained with hematoxylin and eosin (H&E), and finally examined by a digital microscope (Leica QWin). The investigated organs included liver, spleen, kidney, heart and lung.

2.12. Blood analysis

Three healthy Balb/c mice were injected with 200 μL of 100 μM PEGylated NIR712-doped NPs. The other three mice were used as the untreated control. At Day 1, 7 and 14 after NP injection, the mice were sacrificed and blood was collected for blood biochemistry assay and complete blood panel test, which were performed in

Shanghai Research Center for Biomodel Organism.

3. Results and discussion

3.1. Synthesis and characterization of NIR712-doped NPs

NPAFN ONPs with characteristic of aggregation-induced enhanced emission were chosen as encapsulating red-emissive NPs, and a non-water soluble NIR712 was selected as doping NIR dye. The molecular structures of NPAFN and NIR712 are shown in Fig. S1. Reason of the choice is that the photoluminescence (PL) spectrum of NPAFN ONPs overlaps well with the absorption spectrum of NIR712 (Fig. S3), which ensures efficient energy transfer in the guest-host systems and thus leads to enhanced optical properties.

NIR712-doped NPs were prepared by a simple solvent exchanging method [24-25]. Mixtures of NPAFN and NIR712 of different ratios in THF were injected into water under vigorous stirring. Due to a sudden change of solvent environment, NPAFN molecules aggregated and precipitated out to form NPs. During the process, NIR712 molecules were encapsulated into/onto the NPAFN NPs. SEM image (Fig. 1a) shows that the NIR712-doped NPs have roughly spherical structures with an average diameter of about 110 nm. The inset of Fig. 1a shows the TEM image of the NIR-doped NPs. In addition, dynamic laser light scattering (DLS) (Fig. 1b) measurement indicates that the NPs have an average diameter of about 118 nm and narrow size distribution (Polydispersity Index (PDI) = 0.107), which is consistent with the microscopy observation. In order to verify that NIR712 molecules were successfully encapsulated within the host NPs and not easily leaked out, we put the doped NP solution into a 30 k molecular weight cutoff centrifugal membrane, which only allows free NIR712 dyes to pass through. After filtration, the UV-Vis and PL spectra of the filtrate were measured. The results suggest that there were negligible free NIR712 molecules in the filtrate, which indicates that NIR712 molecules were successfully encapsulated into or onto the hydrophobic host material with high stability (Fig. S2).

3.2. Optical properties of NIR712-doped NPs

Upon doping of NIR712, emission from the original NPAFN NPs was effectively quenched and replaced with the emission from NIR712 (Fig. 1d), indicating efficient energy transfer from the host NPs to the dyes. With doping concentration increases, the emission intensity of NIR712 was observed to reach maximum value at a concentration of 0.25% (molar ratio of NPAFN : NIR712 = 1 : 0.25%) and then gradually drop down. At the optimal doping concentration of 0.25% NIR712, the QY is 1.8%.

3.3. The process of energy transfer and amplified fluorescence emission

It was reported that the doping process is a kind of classic föster energy transfer process, which should fit to Stern-Volmer equation $F_0 / F = 1 + K_{SV} * [A]$, where F_0 and F represent the fluorescence intensity in the absence and presence of quencher respectively [26]. The value [A] represents the concentration of the quencher, and K_{SV} is the Stern-Volmer quenching constant, which is obtained from the slope of a linear fit to a plot of F_0/F versus [A]. If the acceptor concentration represents a molecule fraction, K_{SV} indicates the number of host molecules which are quenched by an individual acceptor. Fig. 2a indicates that our experimental results are well in line with the Stern-Volmer equation. The K_{SV} value shows that more than 1000 NPAFN molecules can be quenched by one NIR712 molecule, demonstrating the amplified energy transfer from NPAFN to NIR712. It is shown in Fig. 2b that the fluorescence intensity is greatly enhanced by almost 50 times when excited at 468 nm (~absorption peak of NPAFN) through FRET, in comparison to that obtained by direct excitation at 680 nm (~ absorption peak of NIR712) under the same power density. Such prominent fluorescence amplification is attributed to the light harvesting ability of the NPAFN NPs and the subsequent efficient energy transfer to the doped NIR dyes. The NIR712 doped NPAFN NPs even exhibits 10 times stronger fluorescence than an equivalent amount of free NIR712 in THF solution excited at 680 nm, further indicating the amplified fluorescence emission.

3.4. Surface functionalization of NIR dye-doped NPs

For a practical fluorescent probe, water-dispersibility and bio-environmental stability are essential requirements. We thus functionalized the NIR712-doped NPs with amphipathic surfactant C18PMH-PEG, a common surfactant used in bio-applications [27]. Since the NPs have hydrophobic surface properties, it is convenient that C18PMH-PEG will be anchored to them through hydrophobic interactions. This was confirmed by the comparing the FTIR spectra of NIR712-doped NPs and C18PMH-PEG modified NIR712-doped NPs (Fig. S4a). The figure shows that, after functionalization, the FTIR spectrum presents bands at around 1100 cm^{-1} (indicated by a blue arrow) which are corresponding to the C-O-C stretching modes of PEG, indicating the existence C18PMH-PEG. After functionalization, we systematically studied the size and fluorescence intensity evolution of the NPs in a variety of environments including PBS, serum and solutions with pH = 2-10. Fig. S4b reveals that the size of the functionalized NPs still remained stable in different solutions after even 60 days. They also preserved strong photoluminescence in various environments (Fig. 2c). In marked comparison, the unmodified NPs were easy to aggregate with size significantly increased (Fig. S5a) and the fluorescence intensity quenched accordingly (Fig. S5b) within 30 minutes due to the damage of the surface charges by zwitterions in physiological saline. The total results demonstrate that surface functionalization by C18PMH-PEG can successfully endow the NPs with favorable water dispersibility and stability in various bio-environments, which makes the NPs suitable for *in vitro* and *in vivo* bioimaging. The results of the PL stability also prove that the NIR712 molecules are successfully loaded on the host material.

3.5. Cytotoxicity

Cytotoxicity of cell probes is crucial to their biomedical applications. To evaluate the cytotoxicity of NIR712-doped NPs before and after surface functionalization, standard MTT assays were performed on KB, HeLa and MRC-5 cell lines. As shown

in Fig. 2d and Fig. S6, these cell lines still retain high viabilities which are on average greater than 90% after 24 h incubation with the NPs of varied concentrations ranging from 0.6 to 20 μM, suggesting that the NPs have nearly negligible cell toxicity.

3.6. In vitro targeted cell imaging

The highly fluorescent and stable NIR-emissive NPs were further explored as a biological probe for *in vitro* imaging. To investigate the intracellular localization of the NPs, cells were dually labeled with blue nuclei-specific DAPI and green lysosome-specific Green DND-26. As shown in Fig. 3a, blue, green and red signals represent nuclei, lysosome and the NIR712-doped NPs respectively. It can be found that the fluorescence signal of the NPs is well overlapped with that of lysosome, indicating that NPs probes are primarily distributed in lysosome.

Targeted cell imaging is very helpful to early cancer diagnosis. To achieve specific cancer cell targeting, one approach is to coat NPs with molecules which have strong affinity with the receptors expressed on cancer cells. As is well known, folate receptor (FR) is a widely studied cancer cell probe which is expressed on the surface of many types of cancer cells [28], so next we studied FR-mediated cell targeting. We firstly conjugated FA to the PEG terminals of C18PMH-PEG and then used the product to surface functionalize the NIR712-doped NPs. In the experiment, KB cells cultured in FA-free medium were considered as FR-positive cells because of their high FR expression. For comparison, KB cells cultured in normal medium were used as FR-negative controls because these cells have relatively low FR expression. Both types of KB cells were incubated with C18PMH-PEG and C18PMH-PEG-FA modified NIR712-doped NPs. Subsequently, cellular imaging was investigated using confocal laser scanning microscopy (CLSM) with a 488 nm laser excitation and the fluorescence was collected at wavelengths above 700 nm. In Fig. 3b, a strong red fluorescence is observed in FR-positive KB cells cultured with C18PMH-PEG-FA functionalized NPs, while rather weak signals are detected for FR-negative KB cells incubated with C18PMH-PEG functionalized NPs. Furthermore, when excessive free FA was used to block the FR on the KB cells, the fluorescence signals of the

C18PMH-PEG-FA functionalized NPs significantly dropped. Quantitative measurements from flow cytometry also verified the above phenomena. The fluorescence intensity of C18PMH-PEG-FA functionalized NPs in FR-positive cells was much stronger than that of other groups (Fig. 3c). These results clearly demonstrate the highly specific FR targeting of C18PMH-PEG-FA functionalized NIR712-doped NPs to FR-positive cancer cells.

3.7. Photostability of NIR712-doped NPs

High tolerance to photobleaching is one of the most important properties for a qualified fluorescent probe [16]. Therefore, we examined the photostability of the NIR712-doped NPs and compared with that of fluorescein isothiocyanate (FITC) dye under 488 nm laser illumination with confocal microscopy at same conditions. FITC is one of the most commonly used organic dyes in bioimaging. As shown in Fig. 4a, the green fluorescence of FITC dramatically fades after 2 min continuous laser irradiation and totally disappears after 10 min, owing to its severe photobleaching. In a sharp contrast, the red fluorescence of the doped NPs is still spatially resolved even with 60 min continuous laser irradiation under same recording conditions, although with signal intensity dropping. This result indicates that the NIR712-doped small organic NPs present much higher photostability than FITC.

We further investigated the chemical stability of the doped NPs *in vivo*. Twenty microliters of 100 μM NPs were subcutaneously injected into the back of a Balb/c mouse. *In vivo* fluorescence imaging was carried out by a Maestro EX *in vivo* fluorescence imaging system (CRi, Inc.) and the signals were collected at 700-850 nm. Fig. 4b shows that the fluorescence signal of NPs in the injection site is bright red even at 96 h after subcutaneous injection. The result evidences that FRET in the doped NPs was not interfered by complex biological environment, and the surface functionalization successfully rendered the doped NPs with potent stability in various bio-environments with stable optical properties, which makes *in vivo* bioimaging feasible.

3.8. In vivo imaging and biodistribution

The highly stable and bright NPs were then examined for *in vivo* bioimaging applications. The PEGylated NIR712-doped NPs (200 μL of 120 μM solution for each mouse) were intravenously injected into nude mice bearing KB tumor. Fig. S8 shows the time-dependent *in vivo* fluorescence imaging. There was notable fluorescence signals from the skin initially, however, the tumor site became more intense red and could be gradually distinguished from the autofluorescence of the mouse. At 48 h after injection, the fluorescence of the doped NPs was distinctively bright red and spatially resolved in the tumor site (Fig. 5b), indicating the preferential accumulation of the NPs in the tumor. The capacity of the NPs to selectively mark the tumor with an obvious contrast may be attributed to the combined effect of the bright fluorescence nature of the as-prepared NPs and the passive tumor-targeting delivery of nanomaterials to the tumor by enhanced permeability and retention (EPR) effect [29].

We next investigated the biodistribution profiles of the NPs by imaging a series of organs and the tumor of the mice at various time points after injection. Average fluorescence intensities of organs and tissues were calculated by a semiquantitative biodistribution analysis. Organs from a mouse without NP treatment were used as controls to subtract the autofluorescence background. Fig. 5c and d show that the doped NPs exhibited dominant uptake in the liver (67.5% ID g^{-1}) at 1 h after intravenous injection. From 2 to 24 h, more and more NPs were taken up by tumor sites compared with other organs. At 48h post-injection, high levels of NPs were observed in the tumor (41.9% ID g^{-1}) as well as the reticulo endothelial systems (RES) such as liver (39.3% ID g^{-1}) and spleen (7.6% ID g^{-1}), and only little amount of NPs was observed in intestine (4.2% ID g^{-1}). All results distinctly indicate the potential application of using the doped NPs for *in vivo* imaging.

3.9. Histology, biochemistry and hematology assay

In vivo toxicity assessment of the doped NPs was then evaluated because it is also very important for their practical application. We assessed the systematic toxicity of the NPs by measuring body weight, hematology analysis, and blood biochemical

assay. Nine untreated mice were used as a control. In the experimental group of 9 mice, 200 μL of 100 μM PEGylated NIR712-doped NPs was injected to each. No obvious body weight variation was observed for the mice after NP treatment (Fig. S9) compared with that of the control group. Another group of NP treated mice was sacrificed at Day 1, 7 and 14 for careful necropsy. Five representative organs including liver, kidney, spleen, lung, and heart of the mice were sectioned and stained by hematoxylin and eosin (H&E) for histology analysis (Fig. 6). In spite of relatively high RES uptake of the doped NPs in liver, no noticeable organ damage, inflammation and lesions were observed at Day 1, 7 and 14. Other organs of mice also showed no apparent histopathological abnormalities in comparison with those of the control mice. Histology results provide macroscopic and visual evidence of toxicity. To quantify the toxicity of the doped NPs, another important step is performing serum biochemistry and hematological assay. In the assay, the following standard hematology markers were selected for analysis: white blood cell count (WBC), mean corpuscular volume (MCV), red blood cell count (RBC), hematocrit (HCT), hemoglobin (HGB), mean corpuscular hemoglobin (MCH), mean corpuscular hemoglobin concentration (MCHC), and platelet count (PLT). The results indicate that all measured factors of the NPs were within normal ranges and no apparent abnormalities were observed at Day 1, 7, and 14 (Fig. S10). Next, we measured a variety of factors (alkaline phosphatase (ALP), alanine aminotransferase (ALT), Aspartate aminotransferase (AST), blood urea nitrogen (BUN), creatinine (CRE), total protein (TP)) in the serum to assess liver function, hepatocellular injury, and kidney function. Almost all of the data fell within normal range (Fig. 7), suggesting that no obvious hepatic and kidney disorder of mice be induced by the NP injection. These data indicate that NIR712-doped NPs are not noticeably toxic to mice at the injected dose, which means that they could be a safe fluorescence probe for bioimaging.

4. Conclusions

We have demonstrated an approach of encapsulating NIR dyes into NPAFN NPs

to enable efficient FRET to achieve NIR emission for *in vitro* and *in vivo* imaging. Energy transfer from the host NPAFN NPs to the guest NIR712 molecules render this nanoprobe with large Stokes shift and amplified fluorescence emission. Furthermore, surface modification of the NPs with amphipathic surfactant endows them with water dispersity, stability and biocompatibility in various bio-environments. Last but not least, systematic *in vivo* toxicity studies indicate the favorable biocompatibility of the NIR712-doped ONPs. These superior properties enable the NIR-doped ONPs to be a potential probe for *in vitro* and *in vivo* imaging.

Acknowledgments

This work was supported by National Basic Research Program of China (973 Program, Grant Nos. 2013CB933500, 2012CB932400, 2011CB808400), Major Research Plan of the National Natural Science Foundation of China (No. 91027021, 91233110), and National Natural Science Foundation of China (Nos. 51173124, 51172151). We also thank Natural Science Foundation of Jiangsu Province (No. BK2010003) and a Project Funded by the Priority Academic Program Development of Jiangsu Higher Education Institutions.

Figures and captions

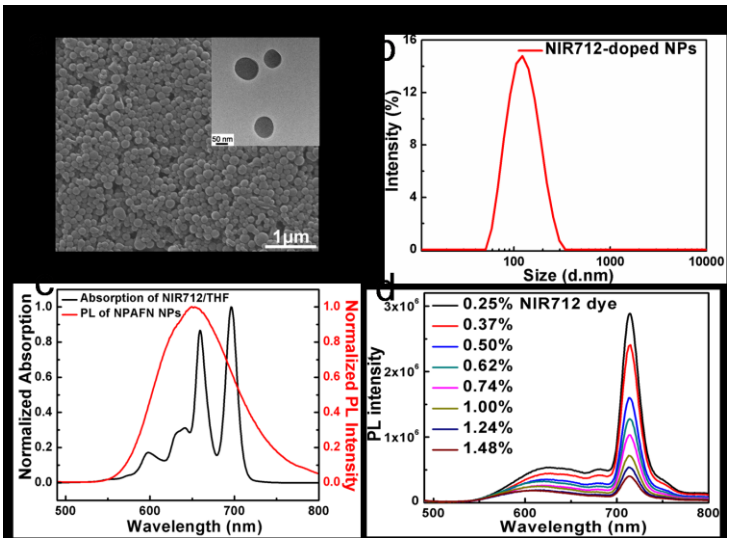

Fig. 1. Characterization of NIR712-doped NPs: (a) SEM and TEM (inset) images; (b) Size distribution of the NPs by DLS measurement at 25 °C in water; (c) Normalized absorption (black line) spectrum of NIR dye/THF and fluorescence emission spectrum (red line) of NPAFN NPs; (d) Fluorescence spectra of NIR712-doped NPs at different doping concentrations.

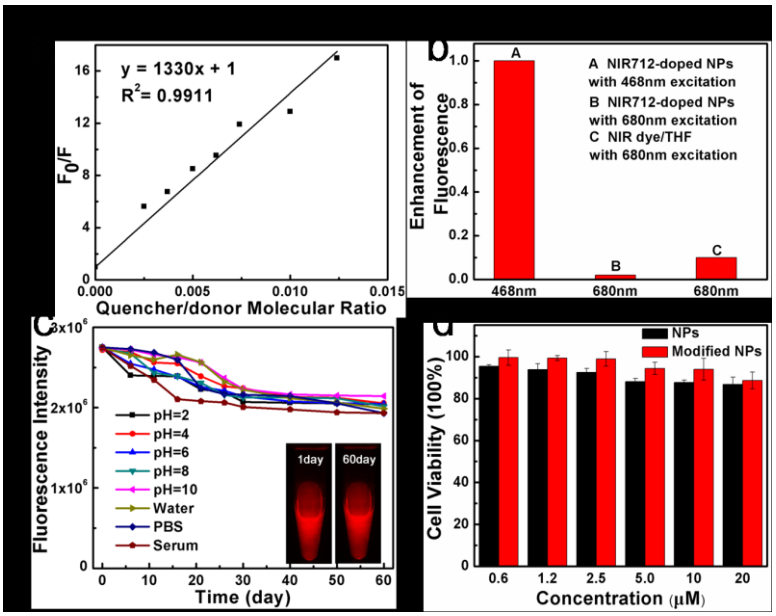

Fig. 2. (a) Fluorescence quenching of donor versus molecule fraction of quenchers in NIR712-doped NPs. The scattered points represent the experimental results of the NPAFN fluorescence quenched by acceptors, and the solid line indicates the fit to the Stern-Volmer equation; (b) Normalized fluorescence peak intensities of NIR712-doped NPs and free NIR712 dye. For NIR712-doped NPs, excitation wavelength was set at 468 nm and 680 nm respectively, while the fluorescence of free NIR dyes was measured in THF with excitation wavelength of 680 nm; (c) Fluorescence intensity studies of NIR712-doped NPs treated with buffer solutions with pH values of 2 to 10, PBS and serum. Inset: fluorescence images of NIR712-doped NPs at Day 1 and Day 60; (d) MTT assay measured viabilities of KB cells incubated with NIR712-doped NPs and C18PMH-PEG modified NIR712-doped NPs of different concentrations for 24 h.

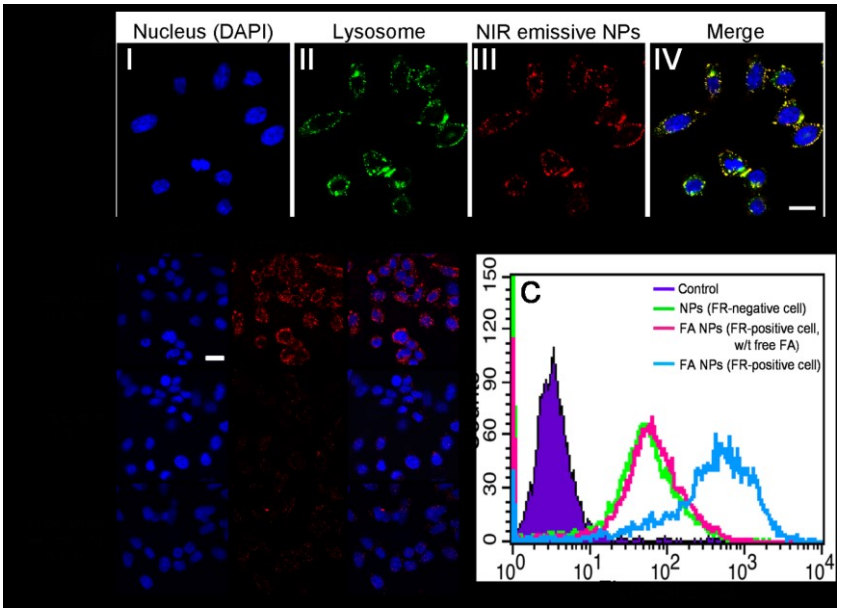

Fig. 3. (a) Confocal laser-scanning fluorescent microscopy images of normal KB cells incubated with (I) DAPI, (II) LysoTracker Green DND-26, (III) NIR712-doped NPs modified with C18PMH-PEG, (IV) Overlay of (I), (II) and (III). The scale bar indicates 20 μm; (b) Confocal laser-scanning fluorescent microscopy images of FR-positive KB cells incubated with NIR712-doped NPs modified with C18PMH-PEG-FA, FR-negative KB cells incubated with NIR712-doped NPs modified with C18PMH-PEG and FR-positive KB cells inhibition FA, then incubated with NIR712-doped NPs modified with C18PMH-PEG-FA respectively. The scale bar is 20 μm; (c) Flow cytometry detection of NIR712-doped NPs-labeled KB cells at same concentration; the colored lines show the fluorescence intensity distributions. Same volume of PBS was used as control group.

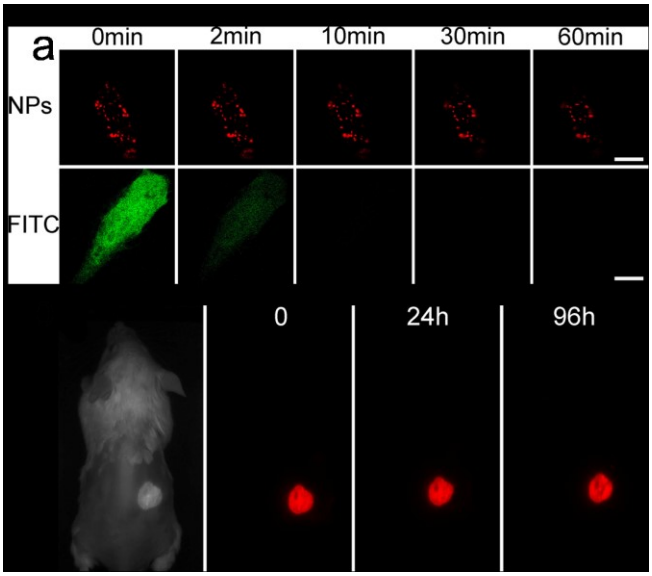

Fig. 4. (a) Fluorescence signals of KB cells labeled by NIR712-doped NPs (red) and FITC (green) at different time points. Scale bars are 10 μm; (b) Bright field picture and fluorescence images of a Balb/c mouse at 0, 24, and 96 h after subcutaneous injection of 20 μL of 100 μM NIR712-doped NPs. All fluorescence images were acquired with 100 ms exposure time.

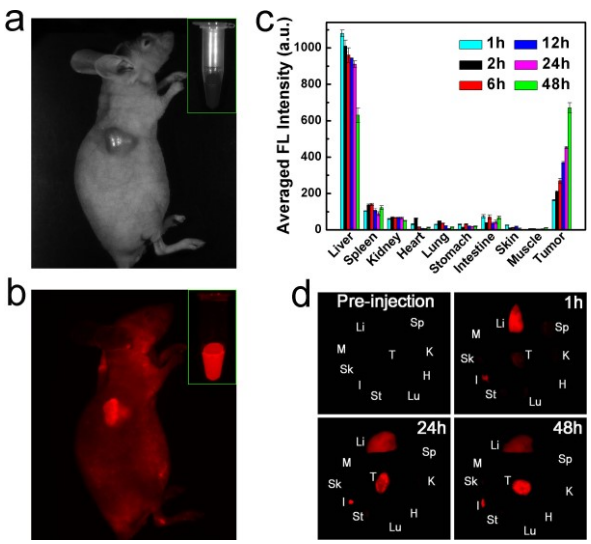

Fig. 5. (a) Bright-field image of a KB-tumor-bearing nude mouse and NIR712-doped NP solution (inset); (b) *In vivo* fluorescence image of a mouse at 48 h after injection of the NIR712-doped NPs with 200 ms exposure time and the NIR712-doped NPs solution with 10 ms exposure time (inset); (c) Semiquantitative biodistribution of the NIR712-doped NPs in mice determined by averaging the fluorescence intensity of each organ; Error bars were calculated from the data of three mice for each group; (d) Spectrally resolved *ex vivo* fluorescence images of organs before injection and at 1, 24, and 48 h after injection of the NIR712-doped NPs. Li: liver, M: muscle, Sk: skin, I: intestine, St: stomach, Lu: lung, H: heart, K: kidney, Sp: spleen, and T: tumor. All fluorescence images were acquired with 200 ms exposure time.

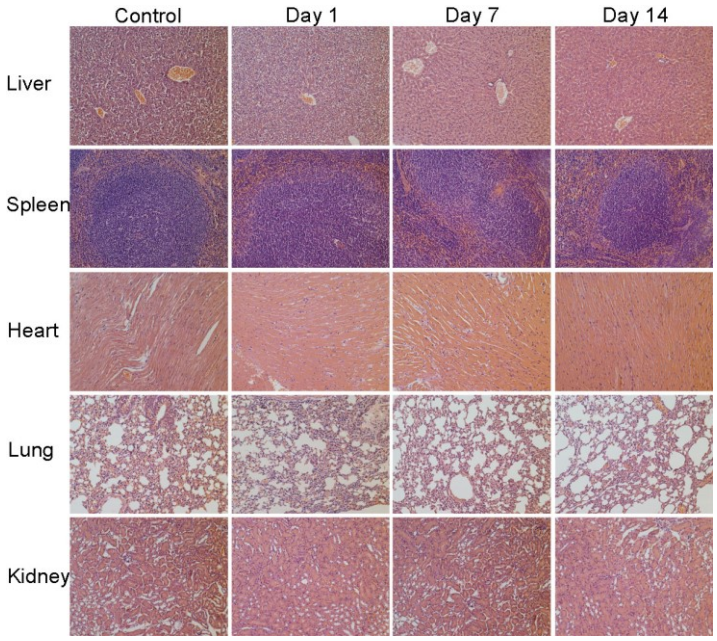

Fig. 6. Liver, spleen, heart, lung and kidney histology images. Organs were stained with haematoxylin and eosin.

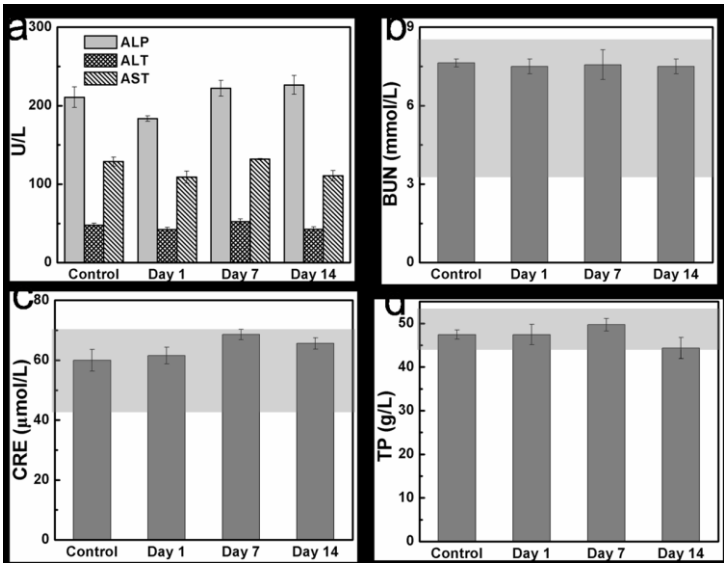

Fig. 7. Serum biochemistry data in blood at various time points after NIR712-doped NP treatment: (a) alkaline phosphatase, alanine aminotransferase, aspartate aminotransferase, (b) blood urea nitrogen, (c) creatinine, (d) total protein. Statistics were based on three mice per data point.

ToC figure

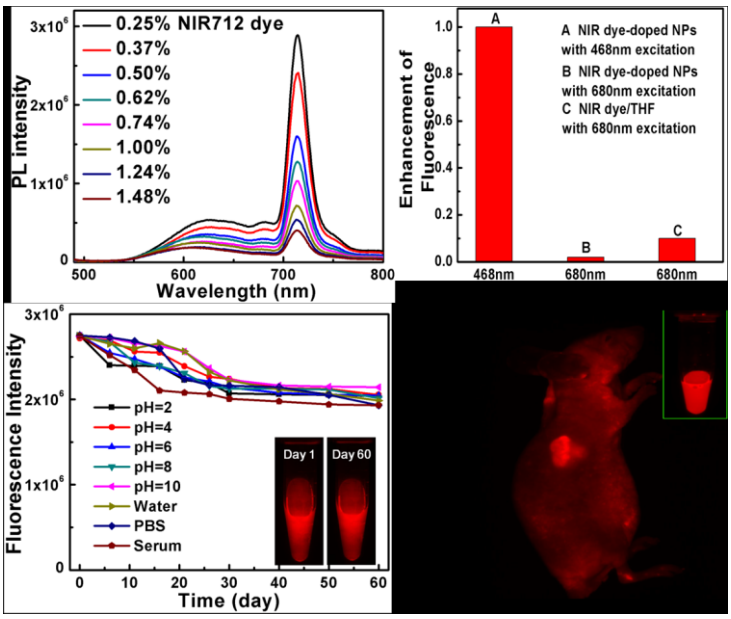

We demonstrated an approach of encapsulating NIR dyes into red-emissive organic nanoparticles to enable efficient FRET and achieve NIR probes with large Stokes shift, amplified fluorescence emission, outstanding photo- and bio-environmental stability, and high biocompatibility for *in vitro* and *in vivo* imaging. All results prove the NIR-doped NPs can be a potential NIR fluorescent probe in biomedical applications.

References

[1] Greenlee RT, Murray T, Bolden S, Wingo PA. Cancer statistics. CA Cancer J Clin 2000;50:7–33.

[2] Frangioni JV. In vivo near-infrared fluorescence imaging. Curr Opin Chem Biol 2003;7:626–34.

[3] Altnolu EI, Adair JH. Near infrared imaging with nanoparticles. Wiley Interdiscip Rev Nanomed Nanobiotechnol 2010; 2:461–77.

[4] Smith AM, Mancini MC, Nie SM. Second window for in vivo imaging. Nat Nanotech 2009; 4:710-1.

[5] Escobedo JO, Rusin O, Lim S, Strongin RM. NIR dyes for bioimaging applications. Curr Opin Chem Biol 2010;14: 64–70.

[6] He XX, Gao JH, Gambhir SS, Cheng Z. Near-infrared fluorescent nanoprobes for cancer molecular imaging: status and challenges. Trends Mol Med 2010;16: 574–83.

[7] Luo SL, Zhang E, Su YP, Cheng TM, Shi CM. A review of NIR dyes in cancer targeting and imaging. Biomaterials 2011;32:7127–38.

[8] Achilefu S. The insatiable quest for near-infrared fluorescent probes for molecular imaging. Angew Chem Int Ed 2010;49:9816–8.

[9] Hayashi K, Nakamura M, Miki H, Ozaki S, Abe M, Matsumoto T, Ishimura K. Near-infrared fluorescent silica/porphyrin hybrid nanorings for in vivo cancer imaging. Adv Funct Mater 2012; 22:3539–46.

[10] Altinoğlu EI, Russin TJ, Kaiser JM, Barth BM, Eklund PC, Kester M, Adair JH. Near-infrared emitting fluorophore-doped calcium phosphate nanoparticles for in vivo imaging of human breast cancer. ACS NANO 2008;2:2075–84.

[11] Zheng CF, Zheng MB, Gong P, Jia DX, Zhang PF, Shi BH, Sheng ZH, Ma YF, Cai LT. Indocyanine green-loaded biodegradable tumor targeting nanoprobes for in vitro and in vivo imaging. Biomaterials 2012;33:5603–9.

[12] Reul R, Tsapis N, Hillaireau H, Sancey L, Mura S, Recher M, Nicolas J, Coll JL, Fattal E. Near infrared labeling of PLGA for in vivo imaging of nanoparticles. Polym Chem 2012;3:694–702.

[13] Hilderbrand SA, Weissleder R. Near-infrared fluorescence: application to in vivo molecular

imaging. Curr Opin Chem Biol 2010;14:71–9.

[14] Kim S, Lim CK, Na J, Lee YD, Kim K, Choi K, Leary JF, Kwon IC. Conjugated polymer nanoparticles for biomedical in vivo imaging. Chem Comm 2010;46:1617–9.

[15] Wu CF, Bull B, Szymanski C, Christensen K, McNeill J. Multicolor conjugated polymer dots for biological fluorescence imaging. ACS NANO 2008;2:2415–23.

[16] Yang YL, An FF, Liu Z, Zhang XJ, Zhou MJ, Li W, Hao XJ, Lee CS, Zhang XH. Ultrabright and ultrastable near-infrared dye nanoparticles for in vitro and in vivo bioimaging. Biomaterials 2012;33:7803–9.

[17] Parthasarathy V, Fery-Forgues S, Campioli E, Recher G, Terenziani F, Blanchard-Desce M. Dipolar versus octupolar triphenylamine-based fluorescent organic nanoparticles as brilliant one- and two-photon emitters for (bio)imaging. Small 2011;7:3219–29.

[18] An BK, Kwon SK, Jung SD, Park SY. Enhanced emission and its switching in fluorescent organic nanoparticles. J Am Chem Soc 2002;124:14410–5.

[19] Yang SM, Lu D, Tian LL, He F, Chen G, Shen FZ, Xu H, Ma YG. Stable water-dispersed organic nanoparticles: preparation, optical properties, and cell imaging application. Nanoscale 2011;3:2261–7.

[20] An FF, Ye J, Zhang JF, Yang YL, Zheng CJ, Zhang XJ, Liu Z, Lee CS, Zhang XH. Non-blinking, highly luminescent, pH- and heavy-metal-ion-stable organic nanodots for bio-imaging. J Mater Chem B 2013;1:3144–51.

[21] Zhang XJ, Zhang XH, Zou K, Lee CS, Lee ST. Controlled synthesis of single crystalline nanoribbons, nanotubes and nanowires from intramolecular charge-transfer organic molecules. J Am Chem Soc 2007;129:3527–32.

[22] Fery-Forgues S. Fluorescent organic nanocrystals and non-doped nanoparticles for biological applications. Nanoscale 2013;5:5828-42.

[23] Kim S, Yoon SJ, Park SY. Highly fluorescent chameleon nanoparticles and polymer films: multicomponent organic systems that combine FRET and photochromic switching. J Am Chem Soc 2012;134:12091-7.

[24] Li W, Yang YL, Wang C, Liu Z, Zhang XJ, An FF, Diao XJ, Hao XJ, Zhang XH. Carrier-free, functionalized drug nanoparticles for targeted drug delivery. Chem Comm 2012;48:8120–2.

[25] Diao XJ, Li W, Yu J, Wang XJ, Zhang XJ, Yang YL, An FF, Liu Z, Zhang XH. Carrier-free,

water dispersible and highly-luminescent dye nanoparticles for targeted cell imaging. Nanoscale 2012;4:5373–7.

[26] Wu CF, Zheng YL, Szymanski C, McNeill J. Energy transfer in a nanoscale multichromophoric system: fluorescent dye-doped conjugated polymer nanoparticles. J Phys Chem C 2008;112:1772–81.

[27] Zhou MJ, Zhang XJ, Yang YL, Liu Z, Tian BS, Jie JS, Zhan XH. Carrier-free functionalized multidrug nanorods for synergistic cancer therapy. Biomaterials 2013;34:8960–7.

[28] Mahon E, Salvati A, Bombelli FB, Lynch I, Dawson KA. Designing the nanoparticle-biomolecule interface for "targeting and therapeutic delivery". J Control Release 2012;161:164–74.

[29] Qin W, Ding D, Liu JL, Yuan WZ, Hu Y, Liu B. Tang BZ. Biocompatible nanoparticles with aggregation-induced emission characteristics as far-red/near-infrared fluorescent bioprobes for in vitro and in vivo imaging applications. Adv Funct Mater 2012;22:771–9.

Supplementary information

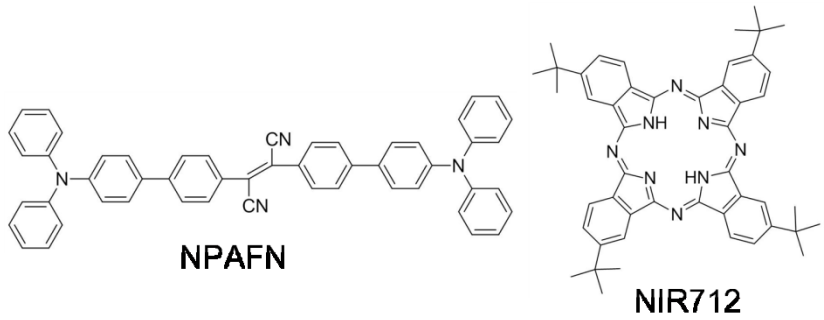

Fig. S1. Molecular structure of NPAFN and NIR712.

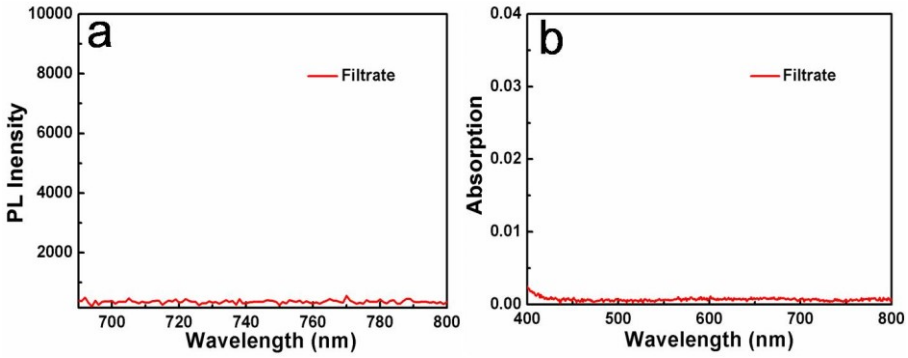

Fig. S2. Emission (λ_{ex} = 680 nm) (a) and absorption (b) spectra of the filtrate.

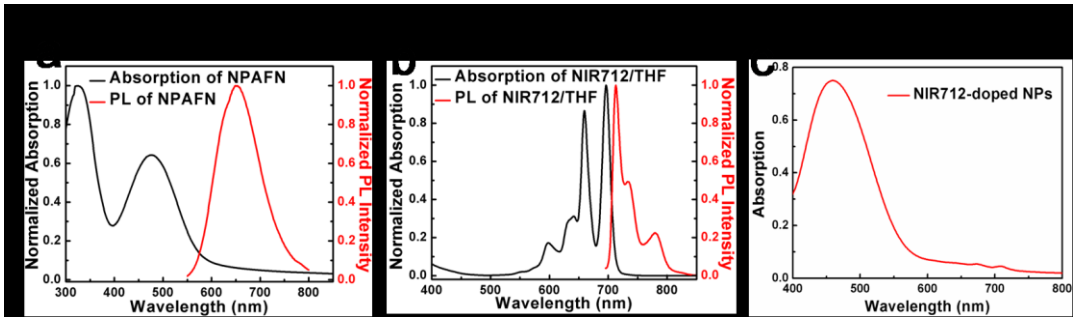

Fig. S3. Normalized absorption (black line) and emission (red line) spectra of NPAFN NPs (λ_{ex} = 488 nm) (a), NIR712/THF (λ_{ex} = 680 nm) (b), and (c) Absorption spectrum of NIR712-doped NPs.

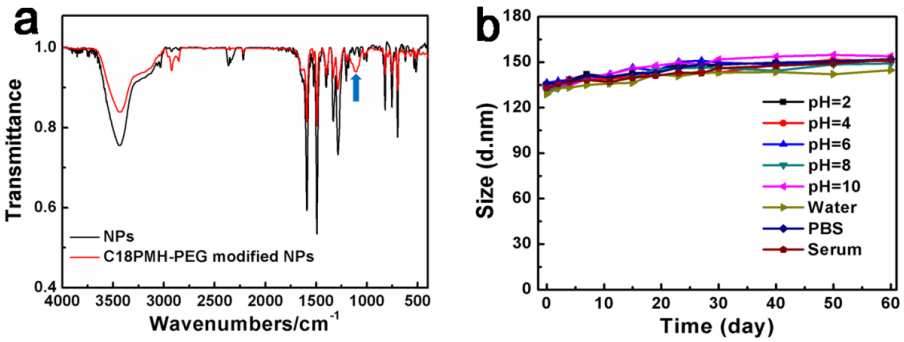

Fig. S4. (a) FTIR spectra of NIR712-doped NPs and C18PMH-PEG modified NIR712-doped NPs; (b) Size studies of modified NIR712-doped NPs treated with serum, PBS, water and buffer solutions with pH values of 2 to 10.

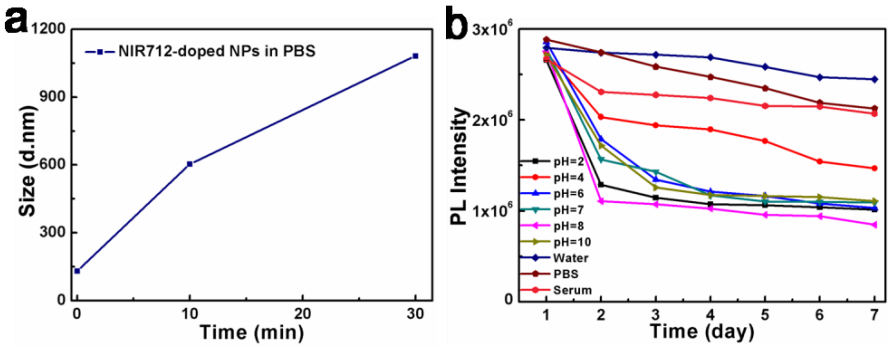

Fig. S5. (a) Size studies of unmodified NIR712-doped NPs in physiological saline within 30 minutes; (b) PL intensity studies of unmodified NIR712-doped NPs treated with serum, PBS, water and buffer solutions with pH values of 2 to 10 within 7 days.

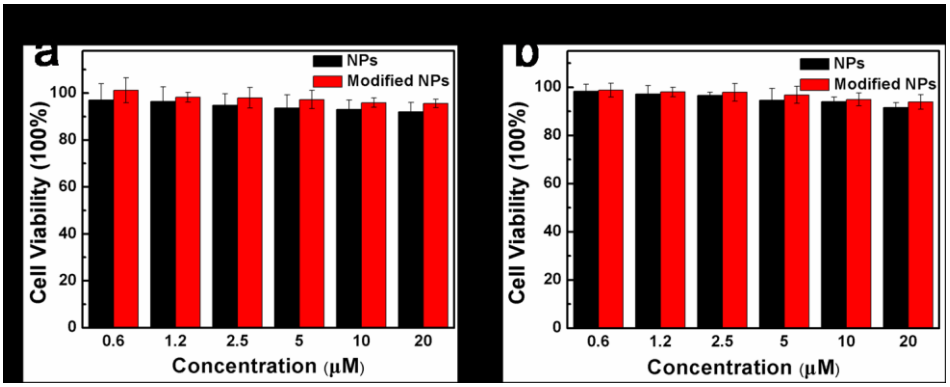

Fig. S6. Viabilities of (a) HeLa cells and (b) MRC-5 cells incubated with NIR712-doped NPs and C18PMH-PEG modified NIR712-doped NPs of different concentrations for 24 h.

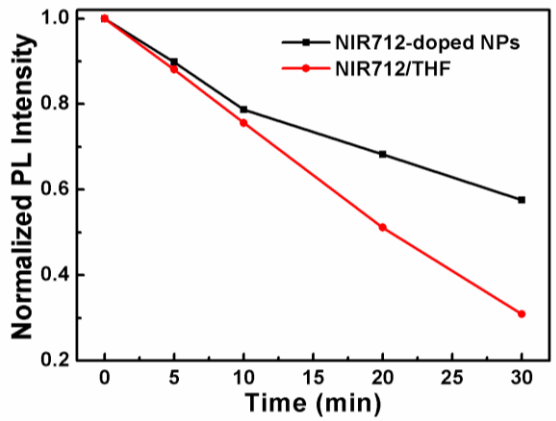

Fig. S7. Photostability of NIR712-doped NPs (in aqueous solution) and NIR712 (in THF). The samples were continuously irradiated by a 300 W xenon lamp. The concentrations of NIR712 remain the same in the two samples. After exposure to a very high density light (300 W xenon lamp and the OD = 0.5 w/cm^2) for approximate 30 min, the fluorescence of NIR712 sharply decreased to about 30%. While in a distinct contrast, the NIR712-doped NPs displayed superior photostability, with the fluorescence intensity only reduced to 60 percent of the initial value within 30 min irradiation. It indicates that the photostability of NIR712-doped NPs is improved compared with NIR712.

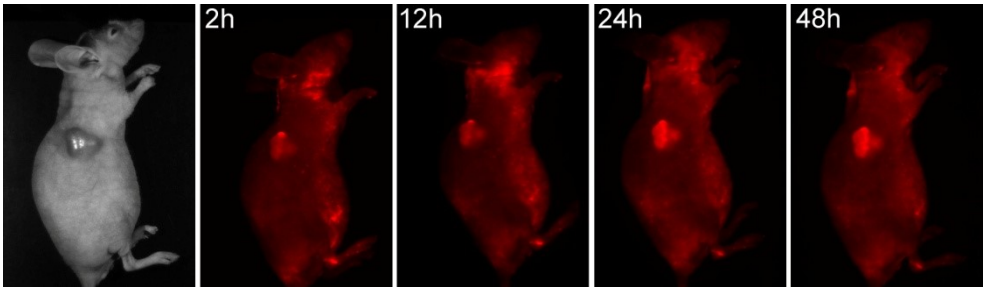

Fig. S8. Bright field image and *in vivo* fluorescence images of a mouse at 2 h, 12 h, 24 h and 48 h after injection of NIR712-doped NPs. All fluorescence images were acquired with 200 ms exposure time.

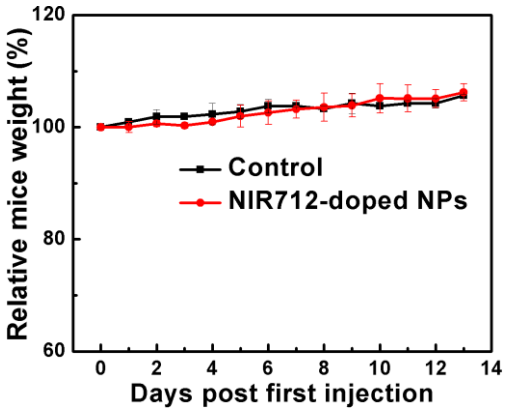

Fig. S9. Normalized body weight curves of mice at different time points post injection. One group of mice was not treated and used as a control. The other group of mice was injected with 200 μL of 100 μM NIR712-doped NPs.

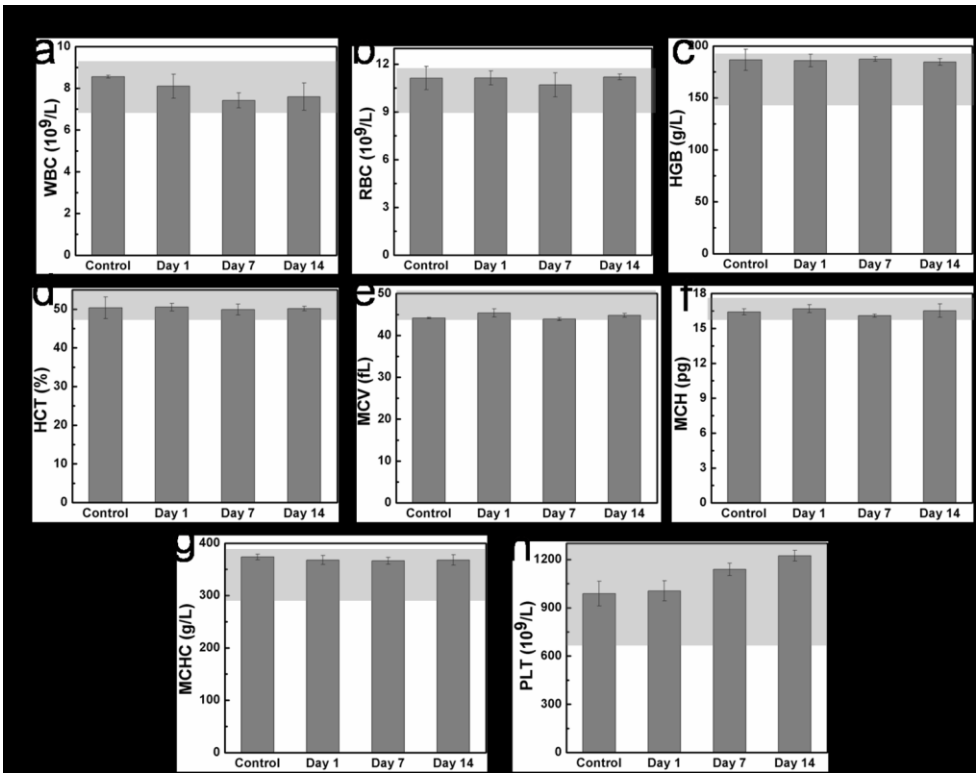

Fig. S10. Healthy female Balb/c mice intravenously injected with NIR712-doped NPs (200 μL of 100 μM) were sacrificed at Day 1, 7 and 14 after injection for blood collection. Untreated healthy mice were used as the control. Hematology results: Blood levels of (a) white blood cells, (b) red blood cells, (c) hemoglobin, (d) hematocrit, (e) mean corpuscular volume, (f) mean corpuscular hemoglobin, (g) mean corpuscular hemoglobin concentration, (h) platelets. Statistics were based on three mice per data point.